Available online at www.sciencedirect.com

ScienceDirect

Geochimica et Cosmochimica Acta 167 (2015) 269–285

Geochimica et Cosmochimica Acta

www.elsevier.com/locate/gca

Petrology and geochemistry of chondrules and metal in NWA 5492 and GRO 95551: A new type of metal-rich chondrite

Michael K. Weisberg [a,b,c,*], Denton S. Ebel [b,c], Daisuke Nakashima [d,e], Noriko T. Kita [d], Munir Humayun [f]

[a] Department of Physical Sciences, Kingsborough Community College, City University New York, Brooklyn, NY 11235, United States
[b] Department of Earth and Environmental Sciences, Graduate Center, City University New York, New York, NY 10016, United States
[c] Department of Earth & Planetary Sciences, American Museum of Natural History, New York, NY 10024, United States
[d] WiscSIMS, Department of Geosciences, University of Wisconsin-Madison, WI 53706, United States
[e] Department of Earth and Planetary Material Sciences, Faculty of Science, Tohoku University, Aoba, Sendai, Miyagi 980-8578, Japan
[f] Department of Earth, Ocean & Atmospheric Science and National High Magnetic Field Laboratory, Florida State University, Tallahassee, FL 32310, United States

Received 12 February 2015; accepted in revised form 14 July 2015; available online 22 July 2015

Abstract

Northwest Africa (NWA) 5492 and Grosvenor Mountains (GRO) 95551 are metal-rich chondrites having silicate (olivine and pyroxene) compositions that are more reduced than those in other metal-rich chondrites, such as the CH and CB chondrites. Additionally, sulfides in NWA 5492 and GRO 95551 are more abundant and not related to the metal, as in the CB chondrites. Average metal compositions in NWA 5492 and GRO 95551 are close to H chondrite metal. Oxygen isotope ratios of NWA 5492 and GRO 95551 components (chondrules and fragments) show a range of compositions with most having $\Delta^{17}O$ values >0‰. Since there is no matrix component, their average chondrule + fragment oxygen isotopic compositions are considered to be representative of whole rock and ($\Delta^{17}O$ values) are sandwiched between the values for enstatite (E) and ordinary (O) chondrites. These data argue for a close relationship between NWA 5492 and GRO 95551 and suggest that they are the first examples of a new type of metal-rich chondrite.

Oxygen isotope ratios of chondrules in NWA 5492 and GRO 95551 show considerable overlap with chondrules in O, E and R chondrites, with average compositions indistinguishable from LL3 chondrules, suggesting considerable mixing between these Solar System materials during chondrule formation and/or that their precursors experienced similar formation environments and/or processes. Another characteristic shared between NWA 5492 and GRO 95551 and O, E and R chondrites is that they are all relatively dry (low abundances of hydrated minerals), compared to many C chondrites and have fewer, smaller CAIs than many C chondrites. (No CAIs were found in NWA 5492 or GRO 95551 but they contain rare Al-rich chondrules.) We suggest that O, E, R and the NWA 5492 and GRO 95551 chondrites are closely related Solar System materials.

1. INTRODUCTION

Since early descriptions of Allan Hills 85085 (e.g., Grossman et al., 1988; Scott, 1988; Weisberg et al., 1988; Wasson and Kallemeyn, 1990), metal-rich (≥20 vol.%),

* Corresponding author at: Department of Physical Sciences, Kingsborough Community College, City University New York, Brooklyn, NY 11235, United States.
E-mail address: mweisberg@kbcc.cuny.edu (M.K. Weisberg).

http://dx.doi.org/10.1016/j.gca.2015.07.021
0016-7037/

matrix-poor chondrites such as the CB and CH chondrites have been among the most perplexing meteorite groups. Their origin and relationship to other chondrites remain open issues. Their chondrules and other components have been interpreted to be highly pristine materials formed either in the early solar nebula (Newsom and Drake, 1979; Weisberg et al., 1990, 1995, 2001; Meibom et al., 1999; Campbell et al., 2001 ;Krot et al., 2001, 2002; Rubin et al., 2003) or as products of late stage protoplanetary collisions (e.g., Wasson and Kallemeyn, 1990; Campbell et al., 2002; Amelin and Krot, 2005; Krot et al., 2005; Fedkin et al., 2015). Study of new metal-rich meteorites with textural similarities to CH or CB chondrites but from different Solar System reservoirs (locations) may provide a better understanding of the origins of these unusual meteorites and their relationship to emerging worlds.

Northwest Africa (NWA) 5492 and Grosvenor Mountains (GRO) 95551 are recently discovered metal-rich chondrite breccias that represent a new oxygen isotope reservoir and possibly a new chondrite (i.e., asteroid) parent body (Friend et al., 2011; Weisberg et al., 2011a, 2012) and thus require further exploration and characterization. Although they have some textural similarity to CB and CH chondrites, such as high metal abundances and occurrence of large cm-size barred olivine (BO) chondrules, their silicates are (with some exceptions) more reduced, sulfides are more common and not associated with the metal, and their metal compositions differ from CB and CH chondrites, showing a closer affinity to H chondrite metal (e.g., Campbell and Humayun, 2003; Humayun and Weisberg, 2012). Initial oxygen isotope ratios indicate that NWA 5492 and GRO 95551 components (chondrules and lithic fragments) plot in a region above the terrestrial fractionation (TF) line, below ordinary chondrite compositions and just above enstatite chondrites in 3-oxygen space (Weisberg et al., 2011a, 2012; Friend et al., 2011) with one rare (barred olivine) component in NWA 5492 plotting near the CR, CB and CH chondrites (Krot et al., 2010; Weisberg et al., 2011a, 2012). Additionally, metal compositions of both NWA 5492 and GRO 95551 plot off the chondritic Co vs. Ni trend observed in CR, CH and CB metal to higher Co (Weisberg et al., 2012), possibly suggesting the onset of parent body equilibration. The whole rock composition of NWA 5492 shows chondritic Ca/Mg and Al/Mg ratios, with a striking depletion in the Mn/Mg ratio, and Fe/Mg and Ni/Mg ratios that are about $2 \times$ CI (Friend et al., 2011).

Here we present results of a petrologic and geochemical study of the chondrules and metal in NWA 5492 and GRO 95551. We present oxygen isotope data on silicates in individual chondrules in both NWA 5492 and GRO 95551. Our goals are to evaluate the relationships of NWA 5492 and GRO 95551 to each other and to other chondrite groups. Additionally, we want to determine whether the CH–CB oxygen isotope signature reported by Weisberg et al. (2012) is common or rare in these meteorites.

Metal composition is another feature that can be used to evaluate affinities with other chondrite groups. The siderophile element abundances of metal in each of the chondrite groups are distinct. Metal in GRO 95551 has been shown to have affinities to ordinary chondrite metal (Campbell and Humayun, 2003). Thus, to examine the relationship of the metal nodules in NWA 5492 to metal in GRO 95551 and other chondrites, we analyzed siderophile elements by LA-ICP-MS. Our goals are to characterize these unusual chondrites in order to assess their origin and relationship to other chondrite groups. Preliminary results were presented in Weisberg et al. (2012) and Humayun and Weisberg (2012).

2. METHODS

Two thin sections of NWA 5492 (−1 and −2) and one of GRO 95551 (, 51) were documented with backscattered electron (BSE) images using a JEOL JSM-6390 scanning electron microscope with a Bruker Quantax Energy Dispersive Spectrometer (EDS), at CUNY, and a Hitachi S4700 Field Emission Gun Scanning Electron Microscope (FEG-SEM), equipped with a Bruker EDS (at the AMNH). The total (thin section) area studied was 414 mm^2 for NWA 5492 and 64 mm^2 for GRO 95551. Wavelength dispersive spectral maps of Si, Al, Mg, Ca, Fe, Ti, S, P, Na and Ni X-ray emission intensity of the two NWA 5492 sections were generated with a Cameca SX100 electron microprobe (at the AMNH). These maps were previously published in Weisberg et al. (2012). These are "stage maps" (moving stage, stationary electron beam). Operating conditions were 15 kV and 40 nA, with a dwell time of 12 ms on one micrometer beam spots spaced 6 μm apart. Modal analysis was based on these elemental X-ray maps of the sections.

Mineral compositions were determined on nominally 1 μm spots using the Cameca SX100 and JEOL Super Probe (Rutgers) electron microprobes. Natural and synthetic standards were chosen based on the compositions of the minerals being analyzed. An accelerating potential of 15 keV and a sample current of 20 nA were used for silicates and 20 keV and 25 nA for metal. Counting times were 20 s on peak, and 10 s on background (off-peak) spectrometer positions. Relative uncertainties (2 sigma), based on counting statistics for major elements (Si, Fe, Mg) are calculated to be <2% and for Ti, Cr, Mn and Ca they are 10%, 10%, 9% and 5%, respectively. Data reductions were carried out using methods described by Pouchou and Pichoir (1991).

Section NWA 5492-2 was analyzed using a New Wave UP193FX excimer laser ablation – inductively coupled plasma – mass spectrometry (LA-ICP-MS) system at the Plasma Analytical Facility, FSU (Humayun et al., 2007; Humayun, 2012). Ten metal nodules, >1 mm in size, were selected for analysis. A spot size of 100 μm, with 60 laser shots (10 Hz, 3-s dwell time), and 2 GW/cm^2 was used for most spots, but one analysis was taken with a line scan using a 50 μm spot size scanned at 10 μm/s.

The CAMECA IMS 1280 ion microprobe at the University of Wisconsin-Madison (WiscSIMS, Kita et al., 2010) was used for the oxygen three-isotope analyses of olivine and pyroxene, the dominant minerals in the chondrules studied. The analytical procedure is very similar to that described in Kita et al. (2010) that uses three Faraday cups

on the multi-collection system for high precision oxygen three-isotope analyses. We used a Cs^+ primary beam of ~4 nA focused to a 15 μm diameter and obtained secondary ^{16}O intensities at $\sim 3 \times 10^9$ count per seconds (cps), which corresponds to ^{17}O intensities at $\sim 1 \times 10^6$ cps. A single spot analysis took ~7 min. Typically ~15 analyses of olivine and low-Ca pyroxene unknowns in chondrules are bracketed by a total of 8 analyses of the San Carlos olivine standard (Fo_{89}, $\delta^{18}O = 5.32‰$ VSMOW; Kita et al., 2010) that was mounted as a polished thin section. The average external reproducibilities of bracketing standard analyses (2SD) were 0.3‰ for $\delta^{18}O$ and 0.5‰ for $\delta^{17}O$ and $\Delta^{17}O$ during the session. A low-Ca pyroxene standard (En_{97}, $\delta^{18}O = 13.31‰$ VSMOW; Kita et al., 2010) was analyzed in the same session for estimating matrix effect between olivine and pyroxene (Kita et al., 2010). The contribution of the tailing of $^{16}O^1H^-$ interference to the $^{17}O^-$ signal was corrected for by the method described in Heck et al. (2010), though the contribution was negligibly small (⩽0.1‰). After SIMS analyses, all SIMS pits were inspected using a SEM to confirm the analyzed positions.

3. RESULTS

3.1. Shock classification of NWA 5492 and GRO 95551

NWA 5492 is reported as having variable degrees of shock with a shock stage ranging from S3 to S5 (Garvie, 2012-Meteoritical Bulletin 99), based on the shock classification scheme of Stöffler et al. (1991). In the NWA 5492 sections we studied, olivine has sharp optical extinction indicating it is S1, essentially unshocked. However, the coexisting pyroxene is darkened due to inclusions of metal and sulfide. Such silicate darkening in chondrites is usually interpreted as due to moderate degrees of shock. The sharp optical extinction in the olivine may be due to post shock annealing which could have healed the shock features of the olivine (e.g., Rubin, 2004). Alternatively the darkening in the pyroxene is the result of reduction and not due to shock.

GRO 95551 is reported as being heavily shocked (Grossman, 1998-Meteoritical Bulletin 82). In the section we studied the olivine has undulatory extinction and planar fractures. This suggest a shock classification of S3.

3.2. Chondrules

We studied the petrology of 28 chondrules and fragments from GRO 95551, 51 and 45 objects from two thin sections of NWA 5492. Oxygen isotope ratios were determined for olivine and pyroxene grains in 20 objects from GRO 95551 and 15 objects from NWA 5492. Some petrologic descriptions of chondrules have been reported previously by Weisberg et al. (2012) and some of those descriptions are reviewed here.

3.3. Textures and mineral assemblages

NWA 5492 and GRO 95551 appear to be breccias composed of chondrules, lithic fragments and metal nodules (Fig. 1a–c; see also Fig. 1 of Weisberg et al., 2012). Chondrules in NWA 5492 (measured in thin section) are commonly 500 μm to 1 mm in size, with some up to 1.8 mm. The average chondrule size is 1.2 ± 0.5 mm Some angular lithic fragments are several mm in size. The section of GRO 95551 that we studied is dominated by a large (1.2 cm) BO chondrule (C27) surrounded by smaller (260 μm to ~2 mm) chondrules, fragments and metal (Fig. 1b). The average chondrule size in GRO 95551 is 900 ± 500 μm. Many of the smaller objects in GRO 95551 have chondrule textures but with irregular outlines and no evidence of once being spherical. Chondrules and fragments in the NWA 5492 and GRO 95551 sections were classified into textural types according to the descriptions and definitions of Gooding and Keil (1981). The chondrule textures in both GRO 95551 and NWA 5492 include porphyritic olivine (PO), porphyritic pyroxene (PP), porphyritic olivine-pyroxene (POP), radial pyroxene (RP), barred olivine (BO), cryptocrystalline (C) and glass-rich PO (these are glass-rich with phenocrysts constituting less than 20% of the chondrule). Of the 45 chondrules and chondrule fragments studied in two sections of NWA 5492, textural types include, 8 C, 2 RP, 2 BO, 11 PO, 2 Al-rich PO, 17 PP, 1 POP and 2 pyroxene-rich angular fragments. Thus, as in most chondrites, porphyritic is the dominant chondrule texture. Noteworthy, however, is that most of the porphyritic chondrules are either dominantly olivine or dominantly pyroxene and there is a lack of the porphyritic olivine-pyroxene chondrules (POP) that dominate carbonaceous (Ebel et al., in press) and ordinary chondrites (Gooding and Keil, 1981; Kita et al., 2010). The two pyroxene-rich angular fragments are exceptionally large (C12 and C13 in NWA 5492-2), do not have typical chondrule textures and do not have any curved surfaces and thus are determined not to be chondrule fragments (see Appendix B and Figs. 2e, f of Weisberg et al., 2012). In addition, NWA 5492-1 contains a lithic fragment with smaller chondrules (~200 μm in size, labeled "1" in the RGB map of Appendix B; Fig. 2k in Weisberg et al., 2012) that have minerals (e.g., olivine is $Fa_{\sim 0.2}$) compositionally similar to those of chondrules in the host chondrite. However, due to its location at the edge of the section we were not able to obtain reliable oxygen isotope compositions on this fragment.

Silicates in some chondrules are peppered with tiny (micron-submicron) blebs of metal suggestive of reduction of Fe from the silicates, e.g. C12 in NWA 5492-1 (Appendix B; Fig. 2d of Weisberg et al., 2012). The large angular fragments in NWA 5492 (C12 and 13 in Appendix B; Fig. 2e, f in Weisberg et al., 2012) are fine-grained intergrowths of enstatite and FeNi metal, similar to textures observed in some E chondrites (e.g., Van Niekirk and Keil, 2011). Some porphyritic and BO chondrules in NWA 5492 have very unusual textures in which metal or sulfide (troilite and daubréelite) is interstitial to the silicates, occurring where chondrule mesostasis would be expected (C12 in NWA 5492-1 in Appendix B and Fig. 2j of Weisberg et al., 2012).

In GRO 95551, the 28 studied objects (chondrules and fragments) include 3 RP, 1 (exceptionally large) BO, 4

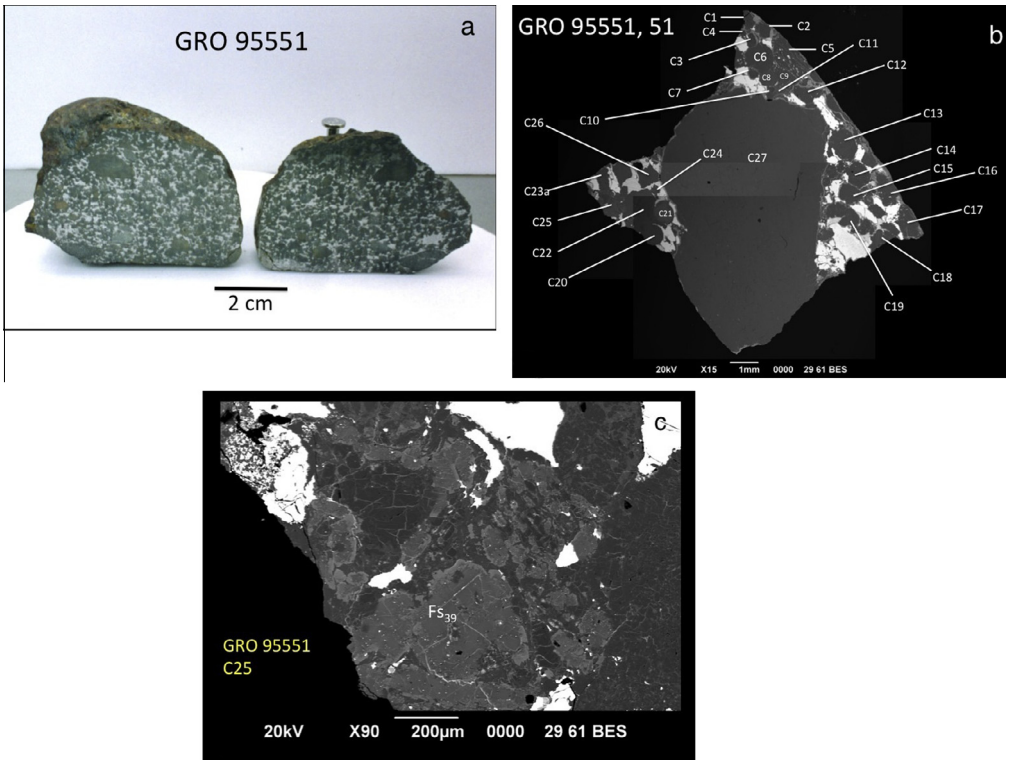

Fig. 1. (a) Photograph of GRO 95551 with cut surfaces showing the high abundance of metal. Photo is courtesy of NASA Johnson Space Center Astromaterials Curation office. (b) Backscatter electron image (BSE) of the thin section of GRO 95551 showing the chondrules that were studied. (c) BSE of C25, a fragment in GRO 95551 that has Fe-rich pyroxene and has an oxygen isotope composition similar to R chondrites.

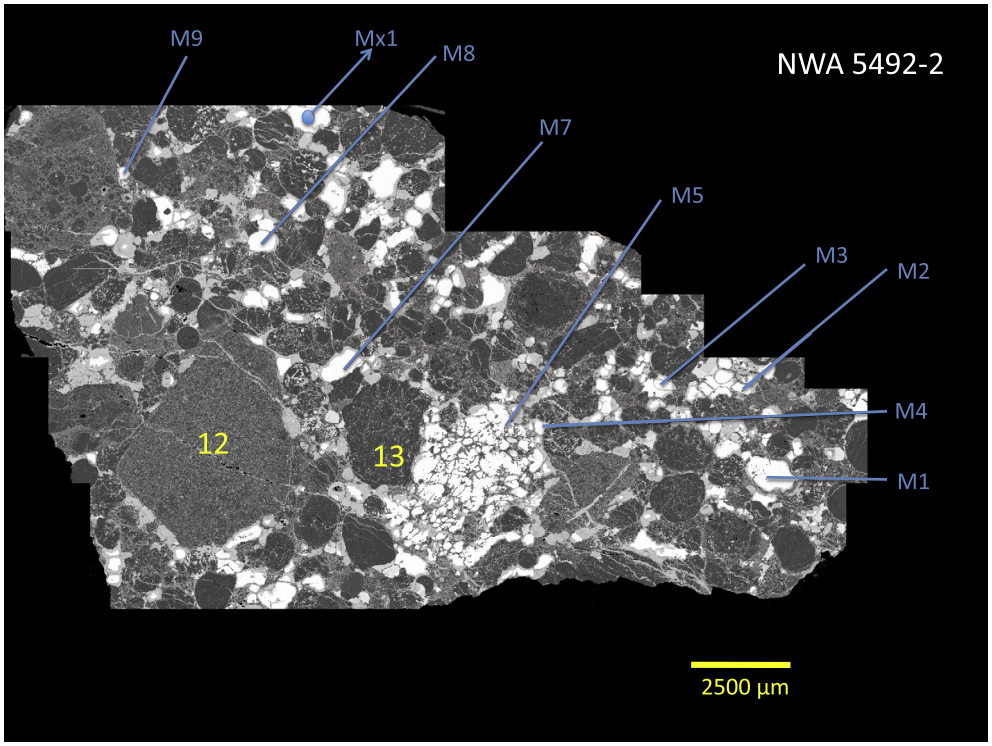

Fig. 2. BSE image of section NWA 5492-2 showing locations of the metal analyzed.

PO, 3 POP, 15 PP and 2 lithic fragments. The two lithic fragments have coarse granular textures not typical of chondrules and one of these (Fig. 1c) has FeO-rich silicate and oxygen isotope compositions similar to R chondrites (as discussed below). As in NWA 5492, some of the silicates in chondrules from GRO 95551 have inclusions of tiny (sub-micrometer-sized) blebs of Ni-poor Fe metal suggesting reduction of Fe from the silicates.

The metal in NWA 5492 occurs as ~500 μm diameter nodules, or clusters of nodules interstitial to the chondrules, or as the mesostasis of some chondrules. The section of GRO 95551 is dominated by a large BO chondrule and thus metal is scarce. However, from the metal we were able to observe in thin section and in images from ANSMET (Fig. 1a), the size and distribution of metal in GRO 95551 seems roughly similar to that in NWA 5492 but no metal was observed as chondrule mesostasis.

3.4. Silicate compositions

Olivine and pyroxene in both NWA 5492 and GRO 95551 chondrules are uniformly highly magnesian (Tables 1 and 2), regardless of chondrule texture. In NWA 5492 average olivine (43 analyses) is $Fa_{0.3}$ with a range of $Fa_{0.1\text{-}0.7}$. Average low-Ca pyroxene (26 analyses) is near-endmember enstatite ($Fs_{0.8}$ $Wo_{0.4)}$ with a range of $Fs_{0.3\text{-}1.6}$ $Wo_{0.3\text{-}0.8}$. (Histograms of olivine and pyroxene endmember compositions were reported in Weisberg et al., 2012.) Average composition (range) of chondrule mesostasis is (wt.%) 61.4 (53.6–64.3) SiO_2, 21.8 (19.2–27.0) Al_2O_3, 4.0 (2.4–8.6) CaO, and 5.9 (2.1–8.6) Na_2O. In GRO 95551, silicates show a wider range in composition. Mean olivine is $Fa_{1.3}$ (21 analyses) with a range of $Fa_{0.7\text{-}3.5}$ and pyroxene ranges $Fs_{0.7\text{-}39.6}$,$Wo_{0.7\text{-}1.6}$. The pyroxene with a composition of $Fs_{39.6}$ is from a single object, C25, see Table 2). Chondrule mesostasis is approximately (wt.%) 41.1–62.5 SiO_2, 20.1–35.7 Al_2O_3, 3.8–19.0 CaO and 0.5–8.1 Na_2O. Data for mesostasis are given as approximations due to concerns about the fine-grained textures of the mesostasis and its possible instability during electron probe analysis.

3.5. Metal compositions

From microprobe analysis, NWA 5492 contains mainly low-Ni metal with a fairly uniform composition. Average (range) metal composition (wt.%) is 5.5 (5.0–5.8) Ni, 0.33 (0.30–0.35) Co, and Cr, P and Si are below detection (<0.03 wt.%), as reported in Weisberg et al. (2012). GRO 95551 has both high-Ni (8.5 wt.%) and low-Ni (4.3 wt.%) metal (Weisberg et al., 2001).

Nine grains from eight metal nodules in NWA 5492-2 were analyzed using LA-ICP-MS, locations for which are shown in Fig. 2. Data are given in Table 3. Preliminary data

Table 1
Average compositions (wt.%) of olivine in chondrules from NWA 5492 and GRO 95551.

Chondrule	SiO_2	TiO_2	Al_2O_3	Cr_2O_3	FeO	MnO	MgO	CaO	Total	Fa (mol.%)	No.
NWA 5492-1											
C1	41.8	0.18	0.10	0.05	0.15	0.12	57.2	0.05	99.6	0.1	16
C4	42.1	bd	bd	0.02	0.17	0.11	57.4	0.01	99.8	0.2	5
C7	43.2	0.03	0.04	0.02	0.14	0.08	57.1	0.06	100.7	0.1	6
C10	43.2	0.04	0.03	0.05	0.69	0.09	57.2	0.07	101.4	0.7	1
C12	42.5	bd	bd	0.00	0.99	0.08	57.0	0.00	100.6	1.0	2
C13	43.4	bd	bd	bd	0.12	0.11	56.8	0.12	100.6	0.1	6
NWA 5492-2											
C1	41.7	bd	bd	bd	0.40	0.16	57.0	bd	99.3	0.4	1
C2	42.0	bd	0.03	0.03	0.20	0.14	56.9	0.04	99.4	0.2	2
C4	41.6	bd	bd	bd	0.40	0.09	57.4	bd	99.5	0.4	5
C5	41.6	0.06	0.07	0.40	0.44	0.10	57.4	0.03	100.1	0.4	4
C13	41.9	0.03	0.06	0.06	0.51	0.11	56.7	0.03	99.4	0.5	1
C18	42.4	bd	bd	bd	0.40	0.09	57.5	bd	100.4	0.4	3
C20	42.3	bd	0.09	0.03	0.38	0.12	57.3	0.08	100.2	0.4	2
C21	42.1	bd	bd	bd	0.30	0.09	57.6	0.04	100.0	0.3	5
C22	42.0	bd	bd	bd	0.21	0.13	57.4	bd	99.7	0.2	3
GRO 95551											
C1	41.5	0.04	bd	0.05	0.87	0.22	57.9	0.09	100.7	0.8	18
C2	41.2	bd	bd	0.07	0.96	0.27	57.8	0.03	100.4	0.9	1
C3	41.6	0.03	0.08	0.06	0.93	0.21	57.7	0.16	100.7	0.9	3
C4	42.1	0.03	0.04	0.05	1.15	0.21	56.2	0.03	99.8	1.1	24
C5	41.8	0.03	bd	0.06	0.99	0.22	56.3	0.08	99.5	1.0	5
C14	42.4	0.07	0.10	0.11	1.04	0.20	56.0	0.19	100.0	1.0	6
C25	42.3	bd	bd	0.03	1.05	0.22	56.4	0.04	100.0	1.0	2
C26	41.7	0.07	0.03	0.06	0.90	0.19	57.2	0.07	100.3	0.9	4
C27	43.1	0.03	0.26	0.08	1.40	0.10	55.2	0.04	100.2	1.4	1

Na_2O and NiO were measured and are below detection (<0.08 and 0.05 respectively) in all pyroxene grains.
bd – below detection (<0.03). No. – number of analyses.

Table 2
Average compositions (wt.%) of low-Ca pyroxene in chondrules from GRO 95551 and NWA 5492.

Chondrule	SiO_2	TiO_2	Al_2O_3	Cr_2O_3	FeO	MnO	MgO	CaO	Total	Wo	FS	No.
NWA 5492-1												
C1	59.8	0.09	0.25	0.09	0.26	0.19	39.4	0.25	100.3	0.5	0.3	2
C4	57.1	0.11	0.54	0.07	0.16	0.13	41.7	0.25	100.1	0.4	0.2	1
C16	59.5	0.04	0.11	0.09	0.21	0.20	39.7	0.27	100.1	0.5	0.3	1
C18	59.7	0.12	0.37	0.07	0.27	0.13	39.5	0.25	100.4	0.5	0.3	5
NWA 5492-2												
C1	58.7	0.07	0.36	0.12	0.49	0.15	39.8	0.25	100.0	0.4	0.7	2
C2	57.8	0.20	1.63	0.45	0.39	0.19	39.0	0.36	100.0	0.7	0.5	2
C4	57.7	0.18	0.96	0.30	0.52	0.14	38.9	0.42	99.1	0.8	0.7	1
C5	58.4	0.19	0.88	0.09	0.89	0.12	40.0	0.29	100.8	0.5	1.3	1
C12	59.0	0.07	0.29	0.07	0.91	0.17	40.2	0.30	101.0	0.5	1.3	2
C13	59.0	0.04	0.17	0.03	1.03	0.17	39.9	0.19	100.6	0.3	1.5	1
C17	59.4	0.07	0.31	0.08	0.40	0.16	40.0	0.27	100.7	0.5	0.5	4
C19	59.4	0.07	0.31	0.08	0.40	0.16	40.0	0.27	100.7	0.5	0.5	1
C20	59.2	0.05	0.24	0.16	0.44	0.23	39.7	0.28	100.3	0.5	0.6	2
C22	58.9	0.09	0.40	0.12	0.19	0.12	39.7	0.22	99.7	0.4	0.3	2
GRO 95551												
C1	58.9	0.10	0.24	0.16	0.70	0.27	40.2	0.27	100.8	0.5	0.9	6
C1	57.1	0.41	1.65	0.30	0.72	0.09	37.9	2.27	100.5	4.1	1.1	7
C2	59.1	0.04	0.18	0.19	0.75	0.27	39.7	0.34	100.5	0.6	1.0	1
C3	57.9	0.16	0.61	0.32	0.90	0.28	39.8	0.51	100.5	0.9	1.2	11
C6	59.4	0.04	0.18	0.31	1.27	0.23	38.6	0.26	100.4	0.5	1.8	20
C7	59.1	0.04	0.14	0.05	0.44	0.17	40.1	0.99	101.0	1.7	0.6	20
C8	57.2	bd	0.07	0.41	6.41	0.18	35.6	0.62	100.6	1.1	9.1	17
C9	58.5	0.06	0.21	0.16	1.11	0.33	38.7	0.38	99.4	0.7	1.6	5
C10	58.5	0.10	0.62	0.31	0.88	0.17	38.2	0.83	99.7	1.5	1.3	3
C11	55.7	0.00	0.18	0.59	11.0	0.64	31.9	0.44	100.5	0.8	16.1	7
C12	58.5	0.07	0.37	0.30	0.65	0.21	38.9	0.38	99.4	0.7	0.9	4
C13	58.3	0.09	0.27	0.19	1.41	0.29	38.5	0.26	99.4	0.5	2.0	5
C15	59.3	0.16	0.56	0.26	1.19	0.26	38.6	0.48	100.9	0.9	1.7	1
C24	58.8	0.07	0.38	0.43	1.80	0.23	38.6	0.35	100.7	0.6	2.6	11
C25	56.8	0.03	0.22	0.47	7.68	0.34	33.8	0.36	99.7	0.7	11.2	1
C25-Fe-pyx	51.8	0.09	0.34	0.12	24.0	0.78	20.6	0.66	98.4	1.4	39.0	1
C27	58.7	0.09	0.31	0.19	0.68	0.28	39.9	0.24	100.4	0.4	1.0	7
C27	55.6	0.28	3.17	0.73	1.96	0.08	36.4	2.37	100.6	4.4	2.8	7

Na_2O and NiO were measured and are below detection (<0.08 and 0.05 respectively) in all pyroxene grains.
bd – below detection (<0.03). No. – number of analyses.

were reported in Humayun and Weisberg (2012). The metal composition of GRO 95551 was reported in Campbell and Humayun (2003). Of the eight nodules in NWA 5492 analyzed, one was dominated by a schreibersite grain (M3). The analysis of one nodule (M5) had silicate contamination as evidenced by the presence of high Si, Ti, V, and Cr, and of Mn, and Zn (not shown). The other six metal nodules were low in Si (<0.05 wt.%), V (<0.4 ppm) and Cr (<6 ppm) implying that the metal was oxidized or sulfidized, unlike metal from CR chondrites (Kong et al., 1999; Humayun, 2012) and CB chondrites (Campbell et al., 2002, 2005). The abundances of Zn (<1 ppm), Mn (<1 ppm), Mo and Sb were also at or below detection limits. For Mo, this was mainly due to a high instrumental blank during that analytical session. Elemental abundances for the 9 nodules are similar so a single average was calculated and is shown in Fig. 3 on a Ni- and CI-normalized plot. Metal in ordinary chondrites varies in its Ni/Fe ratio due to oxidation, and the abundances of most of the siderophile elements correlate with Ni abundance. Thus, we have chosen to normalize the siderophile element abundances to Ni so that elements affected by oxidation (W, Fe, Ga) stand out as anomalies. Further, on a Ni-normalized plot a direct comparison can be made between the siderophile element compositions of bulk chondrites and that of chondritic metal. NWA 5492 metal has a CI chondritic Fe/Ni ratio, but exhibits a small positive Co anomaly due to the presence of troilite and schreibersite that act as additional hosts for Fe and Ni, respectively. Unlike metal from carbonaceous chondrites (e.g., CR, CB), NWA 5492 metal has a fractionated refractory siderophile element pattern similar to those from ordinary and enstatite chondrites, with high W and Re, and low Os, Ir, Pt relative to CI (Fig. 3).

Metal from GRO 95551 shows kamacite-taenite exsolution (Campbell and Humayun, 2003), which introduces additional uncertainty in the bulk GRO 95551 metal composition. The siderophile element pattern of average GRO 95551 metal is shown in Fig. 3, compared with NWA 5492 metal and metal from bulk H chondrite (Kong and

Table 3
Elemental abundances in metal grains from NWA 5492 by LA-ICP-MS.

		M1	M2(a)	M2(b)	M3	M4	M5	M7	M8	Mx1	D.L.
Si	(wt.%)	*0.03*	0.07	0.04	0.66	0.06	0.86	0.03	0.05	0.03	0.03
P	(wt.%)	0.070	0.051	0.057	10.2	0.059	0.380	0.067	0.065	0.072	0.003
S	(wt.%)	0.08	0.11	0.10	0.34	0.10	0.12	0.14	0.09	0.07	0.05
Ti	(ppm)	*13*	*13*	*13*	10	*13*	26	*13*	*13*	*13*	13
V	(ppm)	*0.4*	0.5	*0.4*	0.3	*0.4*	0.9	*0.4*	*0.4*	*0.4*	0.4
Cr	(ppm)	*6*	*6*	*6*	*6*	*6*	21	*6*	*6*	*6*	6
Fe	(wt.%)	94.1	94.1	94.1	63.7	94.2	92.9	94.1	93.9	94.0	
Co	(wt.%)	0.336	0.323	0.326	0.155	0.336	0.315	0.320	0.320	0.321	
Ni	(wt.%)	5.40	5.33	5.34	24.70	5.26	5.39	5.38	5.55	5.45	
Cu	(ppm)	54	53	55	176	53	54	55	55	55	2
Ga	(ppm)	15.2	15.0	15.5	6.0	15.0	14.6	15.5	15.5	14.9	0.2
Ge	(ppm)	26.0	26.7	26.4	11.8	24.9	26.3	26.5	25.9	26.1	0.2
As	(ppm)	4.9	5.0	4.4	3.3	5.1	4.8	4.9	4.8	4.5	1.2
Mo	(ppm)	3	5	3	22	5	3	3	2	1	4
Ru	(ppm)	2.84	3.56	4.13	5.37	3.11	3.26	3.34	3.15	3.11	0.04
Rh	(ppm)	0.53	0.63	0.61	0.54	0.47	0.56	0.61	0.55	0.56	0.01
Pd	(ppm)	2.6	2.5	2.7	5.9	2.7	2.7	2.9	2.6	2.4	0.05
Sn	(ppm)	0.37	0.43	0.40	0.50	0.35	0.35	1.28	0.40	0.37	0.05
Sb	(ppm)	*0.2*	*0.2*	0.2	0.2	0.2	0.2	*0.2*	*0.2*	*0.2*	0.2
W	(ppm)	0.5	0.6	0.6	0.4	0.5	0.6	0.6	0.5	0.6	0.01
Re	(ppm)	0.20	0.17	0.25	0.08	0.22	0.20	0.22	0.18	0.23	0.01
Os	(ppm)	1.81	2.36	2.48	1.19	2.53	2.41	2.42	2.16	2.19	0.001
Ir	(ppm)	1.70	2.06	2.13	1.10	2.35	1.89	2.18	1.92	1.98	0.003
Pt	(ppm)	4.03	4.00	4.45	2.39	4.43	4.26	4.68	4.22	4.29	0.01
Au	(ppm)	0.58	0.73	0.78	1.13	0.66	0.65	0.69	0.66	0.62	0.03

D.L. – detection limit. Values in italics are at the detection limit.

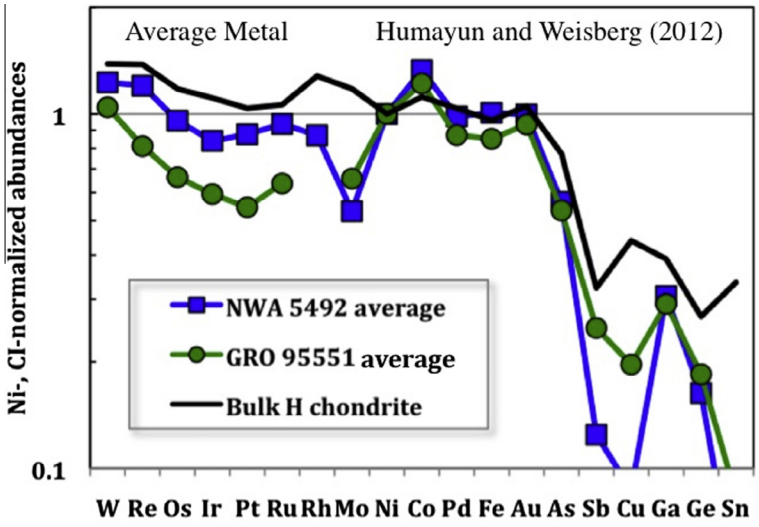

Fig. 3. Elemental abundances of metal (average of eight spots) from NWA 5492 and GRO 95551 (Campbell and Humayun, 2003) compared with bulk H chondrite composition (Kong and Ebihara, 1997; modified by Teplyakova et al., 2012).

Ebihara, 1997). The two metal-rich chondrites have nearly identical metal composition, and it is similar to the siderophile element pattern of bulk H chondrites but lacks the oxidative losses of W, Fe and Ga seen in H chondrite metal (Fig. 3). Thus, metal from NWA 5492 and GRO 95551 could be derived from H chondrite bulk composition by a higher degree of reduction than experienced by ordinary chondrite metal.

3.6. Oxygen isotopes

We made a total of 91 spot analyses in 35 chondrules in NWA 5492 and GRO 95551 (2–6 spots in individual chondrules). Spot locations were checked with SEM and no data were rejected. Images and spot locations for each chondrule analyzed are given in Appendix B (NWA 5492) and A (GRO 95551). Oxygen isotope data for olivine and

pyroxene in NWA 5492 and GRO 95551 chondrules are given in Table 4. The oxygen isotope ratios for NWA 5492 chondrules form a cluster lying mainly between the terrestrial fractionation (TF) and Young–Russell (Y–R) lines (Young and Russell, 1998) in 3-isotope space (Fig. 4a). The data overlap with olivine and pyroxene from chondrules in both enstatite and ordinary chondrites (Kita et al., 2010; Weisberg et al., 2011b). The average deviation of data from the TF line expressed as $\Delta^{17}O$ ($\delta^{17}O - 0.52 \times \delta^{18}O$) is indistinguishable from that of chondrules in LL3 chondrite chondrules (average $\sim +0.5‰$; Kita et al., 2010) and slightly above the TF line ($\Delta^{17}O = 0‰$), as shown in Fig. 5a,b.

Olivine in NWA 5492 and GRO 95551, dominantly from PO (type IA) chondrules, seems to show systematically lower $\delta^{18}O$ values than pyroxene, which are primarily from PP (type IB) chondrules. In Fig. 4d, averages for the NWA 5492 and GRO 95551 chondrules are plotted and sorted by type (IA, IB, IAB). This shows a fairly systematic difference in $\delta^{18}O$ with type IB chondrules generally having higher $\delta^{18}O$ values than type IA. Lower $\delta^{18}O$ values in type IA chondrules relative to type IB chondrules are also seen in LL3 chondrites, and interpreted as a result of evaporation and recondensation during chondrule formation (e.g., Fig. 4 in Kita et al., 2010).

Chondrule C9 in NWA 5492 is an Al-rich (glassy) chondrule with minor olivine and its olivine has the lowest $\Delta^{17}O$ of the chondrules we analyzed (Fig. 4a). Object C12 in NWA 5492-2 is a large (>4 cm) angular fragment consisting mainly of an intergrowth of enstatite and metal, similar to textures described in E chondrites (see Fig. 3 in Weisberg et al., 2012). Two pyroxene grains that were analyzed plot on the TF line toward considerably heavier oxygen values than E chondrites. A third pyroxene from C12 plots closer to the main cluster of pyroxene from the other chondrules (Fig. 4a). Therefore the pyroxene in this object has heterogeneous oxygen isotope ratios that plot on a line on the oxygen-three isotope diagram, but not with a mass-dependent slope. The heterogeneity in the pyroxene may indicate oxygen isotope exchange in this chondrule. Oxygen isotope ratios for GRO 95551 chondrules are similar to NWA 5492 (Figs. 4b,c), but their data are more scattered and the systematic difference in $\delta^{18}O$ values between olivine and low-Ca pyroxene is not so obvious. The overlap in oxygen isotope values supports a close relationship between the two meteorites. Chondrule C27 that dominates our section of GRO 95551 has oxygen isotope ratios that plot on the TF line, similar to some EH3 chondrules (Fig. 4b; Clayton et al., 1984; Weisberg et al., 2011b). Olivine and pyroxene in C25, which has a range of compositions but with the highest FeO content (Fs_{39}), plots above the Y–R line near the range for equilibrated R chondrites (Fig. 4b), suggesting mixing of material from other reservoirs. Note that most $\Delta^{17}O$ values of chondrules in primitive R3 chondrite clasts range from 0‰ to +1.5‰ (Kita et al., 2013), overlapping even more with data from ordinary chondrite (LL3) chondrules as well as GRO 95551 and NWA 5492 chondrules.

The majority of oxygen isotope ratios of the chondrules from NWA 5492 and GRO 95551 show considerable overlap (Fig. 4c). With respect to $\Delta^{17}O$, NWA 5492 and GRO 95551 show a similar range of compositions for the majority of chondrules and they overlap with chondrules from EH3 (Weisberg et al., 2011b) and LL3 (Kita et al., 2010) chondrites (Fig. 5a). However, NWA 5492 and GRO 95551 do not have a matrix component. Thus, the average oxygen isotope ratios of their chondrules plus fragments are essentially equal to whole rock. In comparison to whole rock, the average $\Delta^{17}O$ values for NWA 5492 and GRO 95551 are sandwiched between the O and E chondrites (Fig. 5b).

4. DISCUSSION

4.1. Relationship of NWA 5492 to GRO 95551

GRO 95551 exhibits important similarities to NWA 5492 in texture, mineral composition and oxygen isotope composition, except that silicates in GRO 95551 include a larger range of Fa composition (Weisberg et al., 2012). Oxygen isotope data for individual chondrules show considerable overlap (Fig. 4c). Metal from GRO 95551 exhibits kamacite-taenite exsolution (Campbell and Humayun, 2003), not present in NWA 5492. GRO 95551 and NWA 5492 have nearly identical metal compositions, similar to the siderophile element pattern of H chondrite metal (Fig. 3). Differences in the absolute siderophile element abundances normalized to Ni are dependent on the kamacite-taenite ratio in GRO 95551. Depletions of Mo and Cu are due to partitioning into troilite, while discrepancies at Sb and Sn are not well understood. Overall, the metal from these two chondrites is sufficiently similar in composition to support grouping the two meteorites, consistent with petrologic characteristics and oxygen isotopes.

4.2. A new type of metal-rich chondrite

NWA 5492 and GRO 95551 are metal-rich chondrite breccias with highly reduced silicate compositions unlike any other type of chondrite. Although they are metal-rich (>20 vol.% metal) like CH and contain large metal nodules and large BO chondrules like CB chondrites, their silicate compositions are mainly more reduced and they contain higher abundances of sulfides than CH or CB (Weisberg et al., 2012). Their olivine and pyroxene have near magnesian endmember compositions, similar to those of E chondrites. However, the Si content of the metal is low (below our electron probe detection limit of 0.03 wt.%), unlike metal in the enstatite chondrites (e.g., Keil, 1968; Weisberg and Kimura, 2012). Also, NWA 5492 and GRO 95551 do not contain the array of sulfide minerals that is characteristic of E chondrites, such as oldhamite (CaS), niningerite (MgS) or alabandite (MnS) (e.g., Keil, 1968; Weisberg and Kimura, 2012), but have troilite (FeS) and daubréelite ($FeCr_2S_4$) as their sulfides. Similarities in the oxygen isotope ratios of their components strongly support a close relationship between NWA 5492 and GRO 95551 (Figs. 4 and 5) and equilibration of their components with the same oxygen reservoir. However, mixing of E chondrite (e.g., C12 in NWA 5492) and R chondrite (e.g., C25 in

Table 4
Oxygen isotope compositions of minerals in chondrules from GRO 95551 and NWA 5492.

	Phase	Chondrule Type	$\delta^{18}O$ (‰)	δ^{18} 2σ	$\delta^{17}O$ (‰)	δ^{17} 2σ	$\Delta^{17}O$ (‰)	Δ^{17} 2σ
GRO 95551								
C1–1	Ol	POP	3.36	0.24	2.06	0.46	0.31	0.41
C1–2	Ol		4.13	0.24	2.40	0.46	0.25	0.41
C1–3	Pyx		3.24	0.24	1.76	0.46	0.07	0.41
C2–1	Pyx	PP	5.76	0.25	3.59	0.69	0.59	0.59
C2–2	Pyx		4.96	0.25	2.66	0.69	0.08	0.59
C3–1	Pyx	POP	5.45	0.25	4.22	0.69	1.39	0.59
C3–2	Pyx		5.94	0.25	4.38	0.69	1.29	0.59
C3–3	Ol		4.56	0.25	3.28	0.69	0.90	0.59
C3–4	Ol		5.11	0.25	4.02	0.69	1.36	0.59
C4–1	Ol	PO	5.49	0.24	2.76	0.46	−0.10	0.41
C4–2	Ol		3.71	0.24	1.73	0.46	−0.20	0.41
C4–3	Ol		4.26	0.24	2.01	0.46	−0.21	0.41
C5–1	Ol	PO	4.93	0.15	2.31	0.42	−0.26	0.42
C5–2	Ol		4.49	0.15	2.47	0.42	0.14	0.42
C6–1	Pyx	BP-RP	4.86	0.25	3.20	0.69	0.67	0.59
C6–2	Pyx		5.12	0.25	2.76	0.69	0.10	0.59
C7–1	Pyx	PP	5.55	0.15	3.24	0.42	0.35	0.42
C7–2	Pyx		5.59	0.15	3.50	0.42	0.60	0.42
C8–1	Pyx	PP	3.18	0.15	0.84	0.42	−0.81	0.42
C8–2	Pyx		3.66	0.15	1.15	0.42	−0.75	0.42
C9–1	Pyx	PP	5.06	0.15	3.22	0.42	0.59	0.42
C9–2	Pyx		5.71	0.15	3.22	0.42	0.25	0.42
C10–1	Pyx	PP	4.77	0.15	2.13	0.42	−0.34	0.42
C10–2	Pyx		6.01	0.15	4.04	0.42	0.91	0.42
C11–1	Pyx	PP	3.59	0.15	2.54	0.42	0.68	0.42
C11–2	Pyx		4.29	0.15	3.46	0.42	1.23	0.42
C11–3	Pyx		3.39	0.15	2.67	0.42	0.91	0.42
C11–4	Pyx		3.31	0.15	2.44	0.42	0.72	0.42
C12–1	Pyx	PP	5.15	0.35	2.74	0.63	0.07	0.58
C12–2	Pyx		4.33	0.35	1.93	0.63	−0.33	0.58
C13–1	Pyx	PP	5.75	0.35	4.26	0.63	1.27	0.58
C13–2	Pyx		5.15	0.35	3.63	0.63	0.95	0.58
C14–1	Ol	PO	5.21	0.31	3.55	0.49	0.84	0.54
C14–2	Ol		4.59	0.31	2.84	0.49	0.45	0.54
C14–3	Pyx		4.64	0.31	3.47	0.49	1.06	0.54
C14–4	Ol		4.52	0.31	3.00	0.49	0.65	0.54
C15–1	Pyx	PP	5.73	0.35	3.67	0.63	0.69	0.58
C15–2	Pyx		5.66	0.35	4.01	0.63	1.06	0.58
C21–1	Pyx	POP	6.33	0.31	4.83	0.49	1.54	0.54
C21–2	Ol		4.94	0.31	2.05	0.49	−0.52	0.54
C21–3	Ol		5.10	0.31	2.27	0.49	−0.38	0.54
C21–4	Ol		4.67	0.31	2.28	0.49	−0.15	0.54
C21–5	Pyx		5.57	0.31	2.91	0.49	0.02	0.54
C21–6	Pyx		5.23	0.31	3.36	0.49	0.64	0.54
C23–1	Ol	POP-Frag	3.80	0.31	1.91	0.49	−0.07	0.54
C23–2	Ol		3.38	0.31	2.12	0.49	0.36	0.54
C24–1	Ol	PO	3.36	0.31	2.66	0.49	0.91	0.54
C24–2	Ol		3.35	0.31	2.25	0.49	0.50	0.54
C25–1	Fe-Pyx	Lithic Frag	4.80	0.31	5.47	0.49	2.97	0.54
C25–2	Fe-Pyx		4.85	0.31	5.34	0.49	2.82	0.54
C25–3	Ol		5.10	0.31	5.44	0.49	2.78	0.54
C25–4	Ol		4.93	0.31	4.86	0.49	2.30	0.54
C25–5	Fe-Pyx		3.82	0.35	4.78	0.63	2.80	0.58
C25–6	Fe-Pyx	Lithic Frag	4.95	0.35	5.15	0.63	2.57	0.58
C27–1	Pyx	BO	4.68	0.24	2.47	0.46	0.03	0.41
C27–2	Pyx		5.49	0.24	3.04	0.46	0.19	0.41

(*continued on next page*)

Table 4 (*continued*)

	Phase	Chondrule Type	$\delta^{18}O$ (‰)	δ^{18} 2σ	$\delta^{17}O$ (‰)	δ^{17} 2σ	$\Delta^{17}O$ (‰)	Δ^{17} 2σ
NWA 5492-1								
C4–1	Ol	PO	5.61	0.23	3.99	0.37	1.07	0.34
C4–2	Ol		5.40	0.23	3.13	0.37	0.33	0.34
C4–3	Ol		5.55	0.23	3.99	0.37	1.11	0.34
C4–4	Ol		5.75	0.23	3.32	0.37	0.34	0.34
C4–5	Ol		5.56	0.23	3.74	0.37	0.85	0.34
C7–1	Ol	PO	4.33	0.25	2.71	0.69	0.46	0.59
C7–2	Ol		3.76	0.25	2.12	0.69	0.16	0.59
C10–1	Ol		5.24	0.23	3.63	0.37	0.91	0.34
C10–2	Ol		5.73	0.23	3.86	0.37	0.88	0.34
C12–1	Ol	BO	5.92	0.23	3.69	0.37	0.61	0.34
C12–2	Ol		5.24	0.23	2.90	0.37	0.17	0.34
C13–1	Ol	PO	4.90	0.25	3.41	0.69	0.87	0.59
C13–2	OL		5.23	0.25	3.31	0.69	0.59	0.59
C16–1	Pyx	PP	6.41	0.25	3.98	0.69	0.64	0.59
C16–2	Pyx		6.19	0.25	4.04	0.69	0.82	0.59
C18–1	Pyx	POP	5.99	0.23	3.91	0.37	0.80	0.34
C18–2	Ol		5.00	0.23	3.08	0.37	0.48	0.34
C18–3	Ol		4.90	0.23	3.62	0.37	1.07	0.34
C18–4	Pyx		6.33	0.23	4.00	0.37	0.70	0.34
NWA 5492-2								
C7–1	Ol	PO	5.22	0.25	2.35	0.46	−0.36	0.44
C7–2	Ol		5.62	0.25	3.02	0.46	0.10	0.44
C9–1	Ol	Al-rich	1.88	0.25	0.07	0.46	−0.90	0.44
C9–2	Ol		2.17	0.25	0.51	0.46	−0.62	0.44
C12–1	Pyx	Clast met-sil	6.49	0.25	4.30	0.46	0.93	0.44
C12–2	Pyx		9.48	0.25	4.97	0.46	0.04	0.44
C12–3	Pyx		8.42	0.25	4.64	0.46	0.27	0.44
C13–1	Pyx	Clast met-sil	5.91	0.25	3.55	0.46	0.48	0.44
C13–2	Pyx		5.74	0.25	3.27	0.46	0.29	0.44
C16–1	Pyx	PP	6.34	0.25	4.15	0.46	0.85	0.44
C16–2	Pyx		5.89	0.25	3.64	0.46	0.58	0.44
C17–1	Pyx	PP	5.70	0.25	3.32	0.46	0.35	0.44
C17–2	Pyx		5.84	0.25	3.59	0.46	0.55	0.44
C18–1	Ol	PO	4.86	0.25	3.20	0.46	0.67	0.44
C18–2	Ol		4.90	0.25	3.52	0.46	0.97	0.44
C31–1	Ol	PO	4.94	0.25	3.90	0.46	1.33	0.44

GRO 95551) components and general overlap with the OC field (Figs. 4 and 5) suggest some relationship with the E, O and R chondrites, possibly mixing of the precursor materials during chondrule formation. Interestingly, troilite-dau bréelite-alabandite nuggets (a typical EL chondrite assemblage) have been identified in the Ghubara L5 chondrite, supporting a relationship between E and O chondrites (Ivanova et al., 2000).

In our previous study we reported a clast in NWA 5492 having oxygen isotope ratios similar to CB chondrites (Weisberg et al., 2012). We did not find such ^{16}O-rich oxygen isotope ratios in any of the chondrules from the two thin sections of NWA 5492 analyzed in this study, nor in GRO 95551. We therefore conclude that such clasts are very rare components mixed into the meteorite during brecciation and are not characteristic of the oxygen reservoir for these meteorites. However, we cannot completely exclude the possibility of sampling bias in the sections of NWA 5492 and GRO 95551 that were studied.

The oxygen isotope ratios of most objects in both NWA 5492 and GRO 95551 overlap with chondrules from EH3, LL3 and R3 chondrules. However, with respect to whole rock compositions (assuming that the chondrule average is equal to whole rock), NWA 5492 and GRO 95551 are sandwiched between O and E chondrites. This is especially apparent in their $\Delta^{17}O$ values (Fig. 5). Some chondrules have oxygen isotope ratios that plot on the TF line, similar to E chondrites, e.g., pyroxene from the large BO chondrule C27 in GRO 95551. Oxygen isotope ratios of BO chondrules are thought to represent the composition of the ambient nebular gas because they form by complete melting of their precursors (Clayton et al., 1977; Chaussidon et al., 2008). This suggests a close relationship of NWA 5492 and GRO 95551 to the E chondrites but, based on their average oxygen compositions, textures, metal abundance and mineral compositions, they are a distinct chondrite group. Some of the petrologic and oxygen isotopic characteristics of NWA 5492 and GRO 95551 are summarized and compared to those of other chondrite groups in Table 5.

NWA 5492 and GRO 95551 likely represent a new type of chondrite with affinities to both E and H chondrites. Although there are not enough individual examples of this meteorite type to create a group (5 needed) or grouplet (3 needed), for convenience, we recommend calling them

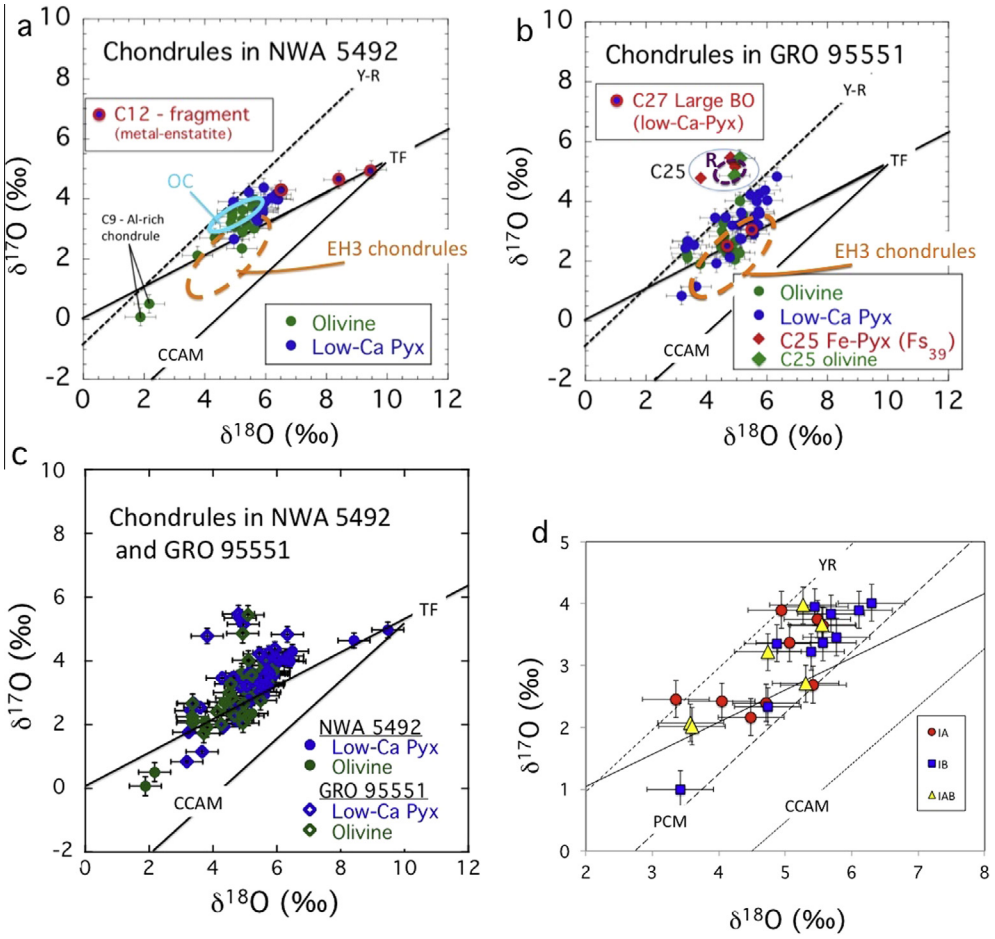

Fig. 4. (a) Oxygen 3-isotope diagram showing oxygen isotope ratios for olivine and pyroxene in NWA 5492 chondrules and fragments. Data cluster mainly between the terrestrial fractionation line (TF) and the Young and Russell line (Y-R) with some data overlapping with ordinary chondrite (OC) whole rock and unequilibrated enstatite chondrite (E3) chondrules. (b) Oxygen isotope ratios for olivine and pyroxene in GRO 95551 chondrules and fragments. Data cluster mainly between the terrestrial fractionation line (TF) and the Young and Russell line (Y-R) with some data overlapping with ordinary chondrite (OC) whole rock and unequilibrated enstatite chondrite (E3) chondrules. Fragment C25 has O isotope ratios similar to R chondrites and C27 (large BO chondrule) has O isotopes ratios that plot on the TF line. (c) Oxygen 3-isotope diagram comparing isotope ratios for the chondrules from NWA 5492 and those in GRO 95551. (d) Oxygen 3-isotope diagram with average ratios for chondrules in NWA 5492 and GRO 95551 sorted by chondrule type. Type IB chondrules tend to have higher $\delta^{18}O$ values than type IA.

"G" chondrites and predict that more examples will be found. The G is for GRO 95551-like chondrites, since GRO 95551 was the first of this type of meteorite to be discovered and described (e.g., Weisberg et al., 2001). Their unique set of characteristics suggest that these meteorites may represent a previously unsampled body from the asteroid belt. Oxygen isotope compositions that plot near the TF line combined with lack of any evidence of hydrous alteration and oxygen isotopic evidence of mixing between O and E reservoirs, all suggest formation of the G chondrites in the inner Solar System and thus, they may be analogues of the materials that accreted to form the terrestrial planets.

4.3. Relationship of NWA 5492 and GRO 95551 to HH and low-FeO ordinary chondrites

Ordinary chondrites more reduced than H chondrites but with similar bulk Fe/Si ratios have been described as a low-FeO OC group (Russell et al., 1998; Troiano et al., 2011). A reduced, metal-rich ordinary chondrite group (HH chondrites) was proposed for Netschaëvo and linked to the parental material of IIE irons (Bild and Wasson, 1977; Wasson and Wang, 1986; Wasson and Scott, 2011). NWA 5492 is a unique chondrite, linked to GRO 95551 (Weisberg et al., 2012), which is both more metal-rich and more reduced than H chondrites but with a similar siderophile element pattern. Indeed, silicates in NWA 5492 (Fa < 1%) are much more reduced than silicates in low-FeO OCs (Fa 13–16; Russell et al., 1998; Troiano et al., 2011), Netschaëvo (Fa_{14}; Bunch et al., 1970), or silicates from IIE irons ($Fa_{14\text{-}17}$; Wasson and Scott, 2011). This is also seen in the Ni content of the metal: NWA 5492 (4.9–5.4%) vs. Netschaëvo (8.6%, Bunch et al., 1970), IIEs (7.2–9.7% Bunch et al., 1970; Wasson and Scott, 2011) and H4–6 metal (8–10%; Kong et al., 1997). Another indication of the state of reduction of the metal is provided by Ga

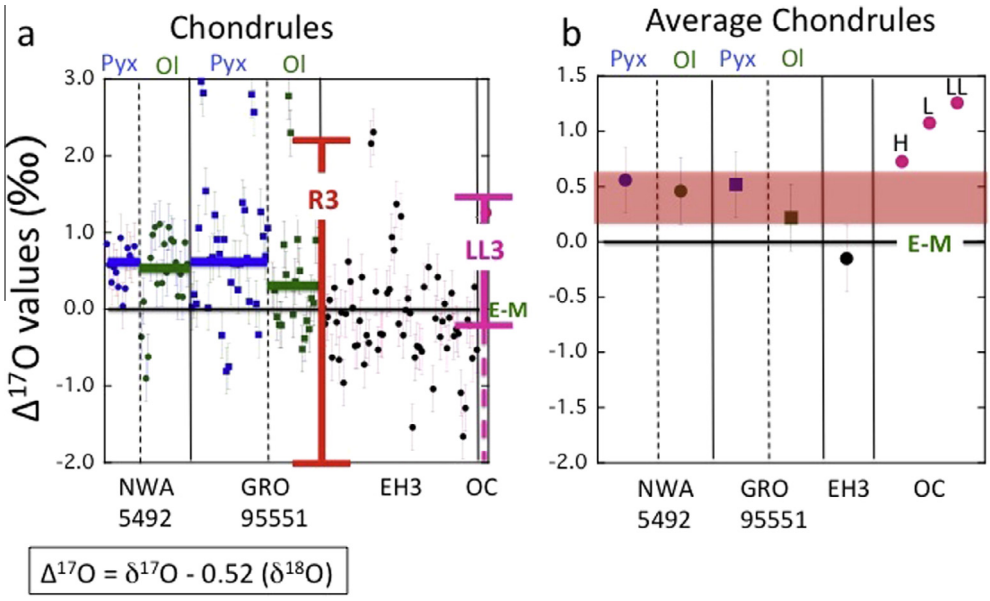

Fig. 5. (a) $\Delta^{17}O$ values for olivine and pyroxene in NWA 5492 and GRO 95551 chondrules compared to values for E3 chondrules and OC whole rock, and showing considerable overlap between the values for all of these materials. Also included are the ranges of values for chondrules in unequilibrated (LL3) ordinary chondrites (Kita et al., 2010) and chondrules R3 chondrite clasts (Kita et al., 2013). (b) Average $\Delta^{17}O$ values for NWA 5492 and GRO 95551 chondrules are similar and are sandwiched between the values for O and E chondrites. NWA 5492 and GRO 95551 have essentially no matrix component so their chondrule + fragment averages are essentially their bulk rock $\Delta^{17}O$ values. Data for E chondrites are from Weisberg et al. (2011b) and ordinary chondrite averages are from Clayton et al. (1991).

abundances which are higher, closer to bulk H chondrite abundances, than the Ga abundances (normalized to Ni and CI) of equilibrated OC metal from H, L, or LL chondrites (Fig. 6a). This implies that the low Cr and V abundances in the metal (a feature also shared by metal from E chondrites) is due to sulfidation of the metal in NWA 5492 rather than due to oxidation (production of chromite), consistent with a higher S content in NWA 5492 than in EOC or CB/CH chondrites. We conclude that NWA 5492 is too reduced to be the parental material of IIEs or to be grouped with Netschaëvo as a member of a new HH chondrite group. The nature of the reductant for NWA 5492 and GRO 95551 and its relationship to the H chondrite parent body is not yet known.

4.4. Metal composition and relationship to the major chondrite groups

NWA 5492 metal does not show the characteristic enrichments of Au and As observed in EL and EH metal (Fig. 3; Kong et al., 1997), but has a CI chondritic Au/Ni ratio, a feature not shared by CR, CH and CB metal that have sub-chondritic Au/Ni ratios. Fig. 6a shows bulk compositions from equilibrated H, L, and LL chondrites (Kong and Ebihara, 1997) compared with metal from NWA 5492. Also shown is the bulk H chondrite composition (Teplyakova et al., 2012). The metal from ordinary chondrites forms a reduction sequence with the elements W, Fe, Ga, and Mo, depleted relative to H chondrites in the sequence LL metal > L metal > H metal > NWA 5492 metal. Metal from NWA 5492 has siderophile element abundances that are nearly identical to H chondrite bulk composition except that Ni, Pd, Fe and Au are ~10–15% higher than most of the other siderophiles. Metal from NWA 5492 lacks the W, Fe, and Ga depletion seen in metal from H4-6 chondrites because it is more reduced. Anomalies in Mo and Cu are due to partitioning into sulfides (Fig. 3).

To examine the reduction sequence further, the $(W/Ni)_{CI}$ ratio is plotted against the $(Fe/Ni)_{CI}$ ratio in Fig. 6b. On this plot, CI chondritic composition plots at unity, CR metal (Kong et al., 1999) plots close by, while bulk H chondrite plots to high $(W/Ni)_{CI}$ ratio ~1.4 × CI, with a chondritic $(Fe/Ni)_{CI}$ ratio. Metal from equilibrated LL, L, H, EL and EH metal plot along a trend of increasing $(W/Ni)_{CI}$ correlated with $(Fe/Ni)_{CI}$ towards the bulk H chondrite composition. Individual metal grains from NWA 5492 plot on a vertical array with eight of the nine nodules defining a constant $(Fe/Ni)_{CI} = 1.01 \pm 0.02$, but exhibiting variable $(W/Ni)_{CI}$ ratios from CI to H chondrite composition. Because W is less siderophile than Fe at $T < 1200$ K (Humayun and Campbell, 2002) metamorphic re-equilibration will cause the $(W/Ni)_{CI}$ ratio to increase. Bulk metal from unequilibrated ordinary chondrites exhibits a $(W/Ni)_{CI}$ ratio that is lower than that of metal from equilibrated ordinary chondrites, and reduction of W from the silicate matrix increases the $(W/Ni)_{CI}$ ratio of metal during equilibration (Humayun and Campbell, 2002).

4.5. Chondrules in NWA 5492 and GRO 95551 compared to other chondrite groups

Chondrules in GRO 95551 are dominantly PP – Type I. In NWA 5492 PO and PP abundances are similar. However, in both NWA 5492 and GRO 95551, the POP textural type appears to be low in abundance.

Table 5
Petrologic and oxygen isotopic characteristics of the G chondrites (NWA 5492 and GRO 95551) compared to those of other chondrite groups.

	CI	CM	CO	CV	CK	CR	CH	CB	H	L	LL	EH	EL	R	K	G
Matrix (vol.%)	>99	60[+]	34	35	50	42	5[++]	<1[++]	12	12	12	8	10	35	73	NF
CAIs abundance (vol.%)	<<1	5	13	10	10	0.5	0.1	<<1	<<1	<<1	<<1	<<1	<<1	NF	<<1	NF
Metal abundance (vol.%)	NF	0.1	1–5	NF–5	NF–5	4–7	22	60–80	10	5	2	10	10	0.1	M	23
Average Chondrule diameter (μm)	NF	0.3	0.15	910	870	700	20	200–10^6	300	400	570	220	550	400	600	1000
Olivine (mol% Fa)	+	+	+	+	<1–47	1–3	2	2.5–4.1	16–20[*]	23–26[*]	27–32[*]	0.4	0.4	38	2.2	0.3–1.3
$\Delta^{17}O$	0.42	−2.29	−4.28	−4.00	−4.15	−1.59	−1.45	−2.29	0.77	1.11	1.22	−0.04	0.06	2.71	−1.55	0.50

NF – not found. M - metal is included in the matrix. Non-G chondrite data are from Rubin (2010) and Weisberg et al. (2008) and references therein, Clayton et al. (1984, 1991, 1999), Weisberg et al. (2001).
[+] Highly variable.
[++] Matrix lumps.
[*] Averages are based on equilibrated meteorites.

Additionally, Type II chondrules, which are common in O chondrites and rare but present in C chondrites, are not found in NWA 5492 or GRO 95551. Thus, the chondrule population in GRO 95551 and NWA 5492 differs from that in O chondrites in which POP are 47–52% of all chondrules (Gooding and Keil, 1981; Nelson and Rubin, 2002) and type II chondrules represent ~50% of chondrules in O chondrites (Kita et al., 2010). Type II chondrules are present but less common (5–10%) in many C chondrites (e.g., Jones, 2012). In CO chondrites, type II chondrules make up 20–25%. The dominance of Type I PP chondrules is similar to that in E3 chondrites (e.g., Weisberg and Kimura, 2012). Additionally, the presence of daubréelite in some chondrules is also like some chondrules in E3 chondrites. However, no Si-bearing metal, oldhamite, niningerite or albandite were found either inside or outside of the chondrules in NWA 5492 and GRO 95551 weakening a direct relationship to E chondrite chondrules. Thus, the observed combination of the abundances of chondrule textural types and mineral assemblage are unique to NWA 5492 and GRO 95551.

The section of GRO 95551 analyzed here is volumetrically dominated by a large BO chondrule, which is superficially similar to the large BO chondrules of some CB chondrites (e.g., Weisberg et al., 2001). Although unusually large, this chondrule is compositionally and isotopically similar to other chondrules in GRO 95551 and NWA 5492. Its oxygen isotope composition falls on the TF line and is similar to the isotopic composition of some EH3 chondrules.

Several porphyritic chondrules in NWA 5492 are unusual in having a mesostasis of FeS and FeCrS or FeNi. This suggests that sulfidation may have played a role in the origin of these chondrules or they formed from melting of sulfide and metal-rich precursors.

Oxygen isotope compositions of the chondrules cluster between and overlap with E and O chondrites, with chondrule averages for NWA 5492 and GRO 95551 very similar to that of LL3 chondrules (analyzed by Kita et al., 2010). Additionally, similar to LL3 chondrules, the type IB chondrules in NWA 5492 and GRO 95551 generally have higher $\delta^{18}O$ values than type IA.

4.6. Lack of matrix in G chondrites

No matrix material was observed in NWA 5492 or GRO 95551. Absence of interstitial matrix is also a characteristic of the CH and CB chondrites (e.g., Weisberg et al., 1995). CH chondrites have matrix-like clasts but no matrix material interstitial to the chondrules and metal. Meibom et al. (2005) found that silicates in some impact melt areas in the QUE 94411 CB chondrite are rich in Fe. They suggested that these areas are the remnants of Fe-rich chondrite matrix material that was once present in the CB chondrites, and that was preferentially melted during impact heating. The lack of interstitial matrix in the G chondrites (NWA 5492 and GRO 95551) could suggest an origin similar to CB chondrites but from a different oxygen reservoir of materials. Lack of matrix could be an indication of rapid hot accretion as suggested by Metzler (2012). Metzler (2012) found that ordinary chondrite breccias contain clasts of what he termed cluster chondrites. These cluster chondrites have chondrules that show plastic deformation and low abundances of matrix and are interpreted to have formed by hot chondrules rapidly accreting after (and during) chondrule formation. Rubin (2010) observed an anti-correlation between matrix abundance and abundances of radial pyroxene and cryptocrystalline chondrules in chondrite groups. Rubin (2010) concluded that this relationship is related to the abundance of dust in local chondrule-forming regions. This relationship may also be related to the efficiency of heating of dust in chondrule-forming environments. In summary, matrix abundance varies widely among chondrite groups

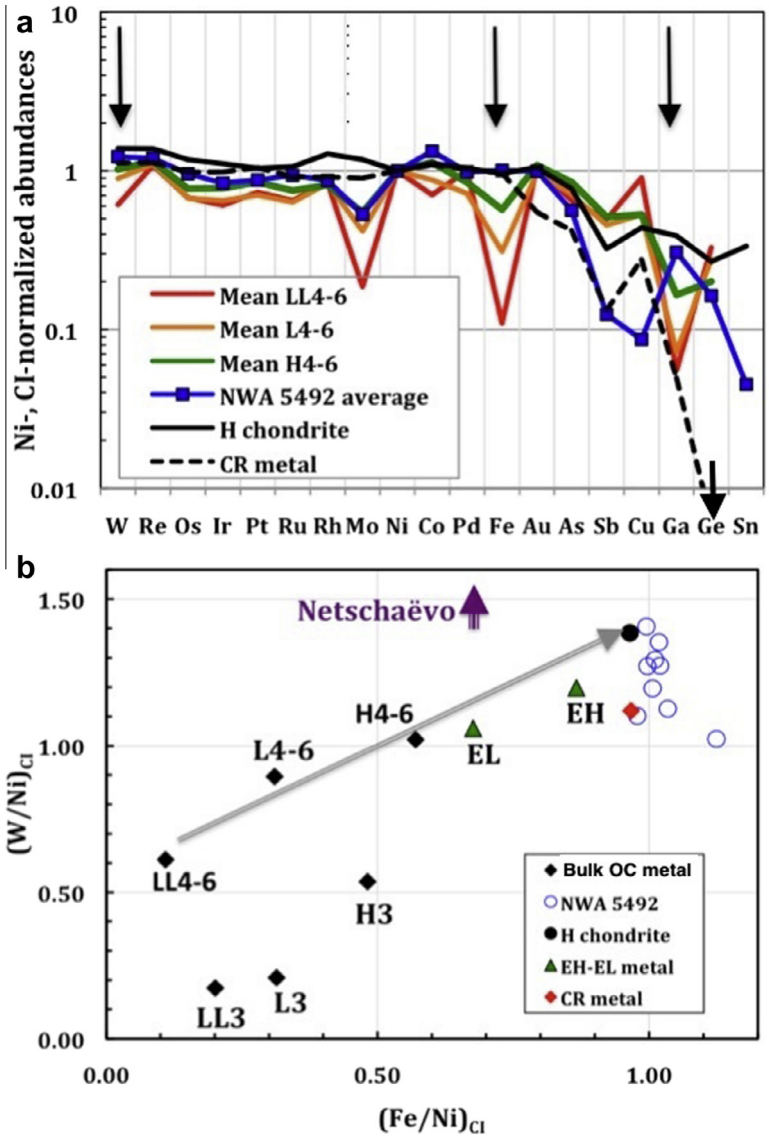

Fig. 6. (a) Siderophile element pattern of NWA 5492 metal compared with metal from equilibrated ordinary chondrites, CR chondrites and bulk H chondrite composition (Kong et al., 1997, 1999; Kong and Ebihara, 1997; Teplyakova et al., 2012). (b) Reduction sequence in equilibrated ordinary chondrite metal (Kong and Ebihara, 1997), E chondrite metal (Kong et al., 1997), compared with metal from NWA 5492, and CR chondrites (Kong et al., 1999). Netschaëvo metal (Wasson and Wang, 1986; Wasson and Scott, 2011) is shown as the purple arrow plotting to $(W/Ni)_{CI}$ ~1.7–2.2. (For interpretation of the references to color in this figure legend, the reader is referred to the web version of this article.)

(Table 5) and may be an important parameter in understanding the evolution of chondrites. However, the cause of this variation is not yet known.

4.7. Relationship between O, E, R and G chondrites

There are several characteristics that O, E, R and G (NWA 5492 and GRO 95551) chondrites have in common. As discussed above there is considerable overlap in the oxygen isotope ratios of O, E and G chondrules (Figs. 3 and 4). Although R chondrites with their high $\Delta^{17}O$ values generally differ, material with R chondrite-like $\Delta^{17}O$ is present in GRO 95551 (Fig. 4b) and a relict grain in a chondrule from an EH3 chondrite has R chondrite oxygen isotope ratios (Weisberg et al., 2011b). Additionally, chondrules in unequilibrated R3 chondrite clasts have $\Delta^{17}O$ values that overlap the range of LL3 chondrite chondrules (e.g., Kita et al., 2013). This suggests mixing of O, E, R and G precursors during chondrule formation and/or during accretion and/or similarities in their formation environments or the processes experienced by their precursors.

E chondrites are characteristically known to have oxygen isotope ratios as well as Cr, Ti, Ni and Zn stable isotope compositions similar to the Earth and Moon (Javoy, 1995; Warren, 2011; Paniello et al., 2012). However, Si isotopes differ (Fitoussi and Bourdon, 2012; Savage and Moynier, 2013). Data for some chondrules in the G chondrites, including the large BO chondrule in GRO 95551, as well

as some chondrules in LL3 chondrites (Kita et al., 2010) are also similar to the Earth-Moon $\Delta^{17}O$ values.

In O, E, R and G chondrites, refractory inclusions are generally small and/or rare, compared to C chondrites. No refractory inclusions have been identified in NWA 5492 or GRO 95551, except for rare Al-rich chondrules. This may indicate that O, E, R and G chondrites formed in a region of the Solar System that received a lower abundance of refractory inclusions or that the refractory component was more thoroughly mixed with chondrule precursors during chondrule formation. This may point to O, E, R and G chondrites forming in a region that is spatial or temporally separated from the C chondrites. The low dust (matrix component) and higher abundance of chondrules in O, E and G, relative to most C chondrites, may indicate that this environment was more efficient in processing (melting and possibly evaporating) dust to form chondrules than that for the C chondrites, and/or more rapid (hot) accretion times for the chondrules and other components in G chondrites (e.g., Metzler, 2012). However, the R chondrites, which have a low abundance of chondrules as do the C chondrites, are inconsistent with this hypothesis. Additionally, Y 82094 is an unusual C chondrite-like meteorite with a low abundance of matrix (Kimura et al., 2014).

Another common feature of the O, E, R and G chondrites is that they are all relatively dry, compared to many C chondrites, with the exception of CK, CH and CB chondrites. CH and CB chondrites are essentially dry but contain hydrated matrix lumps (e.g., Greshake et al., 2002; Ivanova et al., 2008). Although some hydrous minerals have been identified in O and R chondrites, none have been found in E or G. The amounts of hydrated materials in O and R are very minor compared to C chondrites and no O, R, E or G chondrites are considered to be petrologic type 2. The only exception among the E chondrites is the presence of hydrated EC clasts in the Kaidun chondrite breccia (Zolensky et al., 2014).

We conclude that there is a close relationship between O, E, R and G chondrites. Many of their characteristics suggest that they formed in a region separate from the C chondrites. The oxygen (and other stable) isotopic similarities to the Earth and Moon suggest a close relationship to the terrestrial planets. The relatively dry nature of these materials compared to C chondrites suggest they formed inside of the snow line, relatively closer to the sun, where water was primarily in the vapor phase, and ice did not accrete to the parent bodies of these chondrites.

5. CONCLUSIONS

1. NWA 5492 and GRO 95551 are new metal-rich chondrites that are not related to CH or CB based on siderophile element abundances and oxygen isotope compositions. Their silicates are more reduced, their sulfides are more abundant and not intergrown with metal, as in the CB chondrites.
2. Average compositions of metal in NWA 5492 and GRO 95551 are similar and are close to H chondrite metal.
3. Average oxygen isotope ratios of NWA 5492 and GRO 95551 components (chondrules and fragments), show a range of compositions ($\Delta^{17}O = -0.8‰$ to $+3.0‰$) with most having $\Delta^{17}O$ values $>0‰$ sandwiched between the values for whole rock enstatite and ordinary chondrites, with small amounts of R chondrite-like material. The average chondrule + fragment value of NWA 5492 and GRO 95551 are interpreted to represent their whole rock compositions.
4. The similarities in the oxygen isotope ratios of their components strongly support a close relationship between NWA 5492 and GRO 95551.
5. NWA 5492 and GRO 95551 represent a new type of metal-rich chondrite and here are proposed to be the first members of a new (G) chondrite group possibly representing a new chondrite parent body (asteroid).
6. Considerable overlap in oxygen isotope ratios between O, E, R and G chondrules, as well as relict grains of R materials in E and G, suggest that there was considerable mixing between these Solar System materials during chondrule and parent body formation.
7. O, E, R and G chondrites are relatively dry and have fewer, smaller CAIs than C chondrites, but O and G chondrites have Al-rich chondrules. This suggests that the E, R, O and G chondrules were more extensively processed, and the refractory components were integrated into the chondrule population.
8. O, E, R and G chondrites are closely related Solar System materials. Their isotopic similarities to Earth and Moon and low abundance of hydrated minerals suggest that they represent primitive materials from the inner Solar System.

ACKNOWLEDGEMENTS

The authors thank Herbert Palme and Jutta Zipfel for helpful discussions of NWA 5492. We also thank Robert Schenck for technical support. A. Rubin and M. Ivanova are thanked for their thoughtful reviews of the manuscript. The Meteorite Working Group is thanked for approving loan of the GRO 95551, 51 section and Ted Bunch for loaning NWA 5492. This project was supported by NASA Cosmochemistry Grants NNX12AI06G (M. K. Weisberg, P.I.), NNX10AI42G (D. S. Ebel, P.I.), NNX11AG62G (N. T. Kita, P.I.), and NNX13AI06G (M. Humayun, P.I.). WiscSIMS is partly supported by NSF (EAR10-53466).

APPENDICES. SUPPLEMENTARY DATA

Supplementary data associated with this article can be found, in the online version, at http://dx.doi.org/10.1016/j.gca.2015.07.021.

REFERENCES

Amelin Y. and Krot A. E. (2005) Young Pb-isotopic ages of chondrules in CB carbonaceous chondrites. *Lunar Planet. Sci. 36*. Lunar Planet. Inst., Houston, # 1247 (abstr.).

Bild R. W. and Wasson J. T. (1977) Netschaëvo: A new class of chondritic meteorite. *Science* **197**, 58–62.

Bunch T. E., Keil K. and Olsen E. (1970) Mineralogy and petrology of silicate inclusions in iron meteorites. *Contrib. Mineral. Petrol.* **25**, 297–340.

Campbell A. J. and Humayun M. (2003) Formation of metal in GRO 95551 and comparison to ordinary chondrites. *Geochim. Cosmochim. Acta* **67**, 2481–2495.

Campbell A. J., Humayun M., Krot A. and Keil K. (2001) Origin of zoned metal grains in the QUE 94411 chondrite. *Geochim. Cosmochim. Acta* **65**, 163–180.

Campbell A. J., Humayun M. and Weisberg M. K. (2002) Siderophile element constraints on the formation of metal in the metal-rich chondrites Bencubbin, Gujba and Weatherford. *Geochim. Cosmochim. Acta* **66**, 647–660.

Campbell A. J., Humayun M. and Weisberg M. K. (2005) Compositions of unzoned and zoned metal in the CB_b chondrites Hammadah al Hamra 237 and Queen Alexandra Range 94627. *Meteorit. Planet. Sci.* **40**, 1131–1148.

Chaussidon M., Libourel G. and Krot A. N. (2008) Oxygen isotopic constraints on the origin of magnesian chondrules and on the gaseous reservoir in the early solar system. *Geochim. Cosmochim. Acta* **72**, 1924–1938.

Clayton R. N., Onuma N., Grossman L. and Mayeda T. K. (1977) Distribution of the presolar component in Allende and other carbonaceous chondrites. *Earth Planet. Sci. Lett.* **34**, 209–224.

Clayton R. N., Mayeda T. K. and Rubin A. E. (1984) Oxygen isotopic compositions of enstatite chondrites and aubrites. *J. Geophys. Res.* **89**, C245–C249.

Clayton R. N., Mayeda T. K., Goswami J. N. and Olsen E. J. (1991) Oxygen isotope studies of ordinary chondrites. *Geochim. Cosmochim. Acta* **55**, 2317–2337.

Clayton R. N., Mayeda T. K. and Rubin A. E. (1999) Oxygen isotopic compositions of carbonaceous chondrites. *Geochim. Cosmochim. Acta* **63**, 2089–2104.

Ebel D. S., Brunner C., Leftwich K., Erb I., Lu M., Konrad K., Rodriguez H., Friedrich J. M. and Weisberg M. K. (2014) Abundance, composition and size of inclusions and matrix in CV and CO chondrites. *Geochim. Cosmochim. Acta*, (in press).

Fedkin A. V., Grossman L., Humayun M., Simon S. B. and Campbell A. J. (2015) Condensates from vapor made by impacts between metal-, silicate-rich bodies: comparison with metal and chondrules in CB chondrites. *Geochim. Cosmochim. Acta* **164**, 236–261.

Fitoussi C. and Bourdon B. (2012) Silicon isotope evidence against an enstatite chondrite Earth. *Science* **335**, 1477–1480.

Friend P., Zipfel J., Gellissen M., Kleinschrod R., Muenker C., Pack A., Schulz T., Stracke A. and Palme H. (2011) Northwest Africa 5492: An extremely reduced chondritic meteorite with low volatile element contents. 42nd Lunar Planet. Sci., Lunar Planet. Inst., Houston. #1095 (abstr.).

Garvie L. A. J. (2012) The Meteoritical Bulletin, No. 99. http://www.lpi.usra.edu/meteor/docs/mb99.pdf.

Gooding J. L. and Keil K. (1981) Relative abundances of chondrule primary textural types in ordinary chondrites and their bearing on conditions of chondrule formation. *Meteoritics* **16**, 17–43.

Greshake A., Krot A. N., Meibom A., Weisberg M. K. and Keil K. (2002) Heavily-hydrated matrix lumps in the CH and metal-rich chondrites QUE 94411 and Hammadah al Hamra 237. *Meteorit. Planet. Sci.* **37**, 281–293.

Grossman J. N. (1998) The Meteoritical Bulletin, No. 82. *Meteorit. Planet. Sci.* **33**, A221–A239.

Grossman J. N., Rubin A. E. and MacPherson G. J. (1988) ALH85085; a unique volatile-poor carbonaceous chondrite with possible implications for nebular fractionation processes. *Earth Planet. Sci. Lett.* **91**, 33–54.

Heck P. R., Ushikubo T., Schmitz B., Kita N. T., Spicuzza M. J. and Valley J. W. (2010) A single asteroidal source for extraterrestrial Ordovician chromite grains from Sweden and China: high-precision oxygen three-isotope SIMS analysis. *Geochim. Cosmochim. Acta* **74**, 497–509.

Humayun M. (2012) Chondrule cooling rates inferred from diffusive profiles in metal lumps from the Acfer 097 CR2 chondrite. *Meteorit. Planet. Sci.* **47**, 1191–1208.

Humayun M. and Campbell A. J. (2002) The duration of ordinary chondrite metamorphism inferred from tungsten microdistribution in metal. *Earth Planet. Sci. Lett.* **198**, 225–243.

Humayun M. and Weisberg M. K. (2012) A possible ordinary chondrite affinity for metal from the unique chondrite NWA 5492. *43rd Lunar Planet. Sci.*, Lunar Planet. Inst., Houston., # 1458 (abstr.).

Humayun M., Simon S. B. and Grossman L. (2007) Tungsten and hafnium distribution in calcium-aluminum inclusions (CAIs) from Allende and Efremovka. *Geochim. Cosmochim. Acta* **71**, 4609–4627.

Ivanova M. A., Kononkova N. N. and Nazarov N. A. (2000) Rutile and Mn-rich chromite-bearing sulfide nuggets in an unusual inclusion from the Ghubara L5 chondrite. *31st Lunar Planet. Sci.*, Lunar Planet. Inst., Houston., #1715 (abstr.).

Ivanova M. A., Moroz L. V., Kononkova N. N. (2008) Altered material in CH/CB chondrite Isheyevo. 40th Lunar and Planetary Science Conference, 1259.

Javoy M. (1995) The integral enstatite chondrite model of the earth. *Geophys. Res. Lett.* **22**, 2219–2222.

Jones R. H. (2012) Petrographic constraints on the diversity of chondrule reservoirs in the protoplanetary disk. *Meteorit. Planet. Sci.* **47**, 1176–1190.

Keil K. (1968) Mineralogical and chemical relationships among enstatite chondrites. *J. Geophys. Res.* **73**, 6945–6976.

Kimura M., Barrat J. A., Weisberg M. K., Imae N., Yamaguchi A. and Kojima H. (2014) Petrology and bulk chemistry of Yamato-82094, a new type of carbonaceous chondrite. *Meteorit. Planet. Sci.* **49**, 346–357.

Kita N. T., Nagahara H., Tachibana S., Tomomura S., Spicuzza M. J., Fournelle J. H. and Valley J. W. (2010) High precision SIMS oxygen three isotope study of chondrules in LL3 chondrites: role of ambient gas during chondrule formation. *Geochim. Cosmochim. Acta* **74**, 6610–6635.

Kita N. T., Tenner T. J., Ushikubo T., Nakashima D., and Bischoff A. (2013) Primitive chondrules in a highly unequilibrated clast in NWA 753 R chondrite. Lunar Planet. Sci., Lunar Planet. Inst., Houston. 44, # 1784 (abstr.).

Kong P. and Ebihara M. (1997) The origin and nebular history of the metal phase of ordinary chondrites. *Geochim. Cosmochim. Acta* **61**, 2317–2329.

Kong P., Mori T. and Ebihara M. (1997) Compositional continuity of enstatite chondrites and implications for heterogeneous accretion of the enstatite chondrite parent body. *Geochim. Cosmochim. Acta* **61**, 4895–4914.

Kong P., Ebihara M. and Palme H. (1999) Distribution of siderophile elements in CR chondrites: evidence for evaporation and recondensation during chondrule formation. *Geochim. Cosmochim. Acta* **63**, 2637–2652.

Krot A. N., Meibom A., Russell S. S., Alexander C. M. O'D., Jeffries T. E. and Keil K. (2001) A new astrophysical setting for chondrule formation. *Science* **291**, 1776–1779.

Krot A. E., Meibom A., Weisberg M. K. and Keil K. (2002) The CR chondrite clan: implications for early solar system processes. *Meteorit. Planet. Sci.* **37**, 1451–1490.

Krot A. N., Amelin Y., Cassen P. and Meibom A. (2005) Young chondrules in CB chondrites from a giant impact in the early Solar System. *Nature* **436**, 989–992.

Krot A. E., Nagashima K., Yoshitake M. and Yurimoto H. (2010) Oxygen isotopic compositions of chondrules from the metal-rich chondrites Isheyevo (CH/CB_b), MAC 02675 (CB_b) and QUE 94627 (CB_b). *Geochim. Cosmochim. Acta* **74**, 2190–2211.

Meibom A., Righter K., Chabot N., Dehn G., Antignano A., McCoy T. J., Krot A. N., Zolensky M. E., Petaev M. I. and Keil K. (2005) Shock melts in QUE 94411, Hammadah al Hamra 237, and Bencubbin: Remains of the missing matrix? *Meteorit. Planet. Sci.* **40**, 1377–1391.

Meibom A., Petaev M. I., Krot A. K., Wood J. A. and Keil K. (1999) Primitive FeNi metal grains in CH carbonaceous chondrites formed by condensation from a gas of solar composition. *J. Geophys. Res.* **104**, 22053–22059.

Metzler K. (2012) Ultra rapid chondrite formation by hot accretion? Evidence from ordinary chondrites. *Meteorit. Planet. Sci.* **47**, 2193–2217.

Nelson V. E. and Rubin A. E. (2002) Size-frequency distributions of chondrules and chondrule fragments in LL3 chondrites: implications for parent-body fragmentation of chondrules. *Meteorit. Planet. Sci.* **37**, 1361–1376.

Newsom H. E. and Drake M. J. (1979) The origin of metal clasts in the Bencubbin meteoritic breccia. *Geochim. Cosmochim. Acta* **43**, 689–707.

Paniello R., Day J. M. D. and Moynier F. (2012) Zn isotopic evidence for the origin of the Moon. *Nature* **490**, 376–379.

Pouchou J. L. and Pichoir F. (1991) Quantitative analysis of homogeneous or stratified microvolumes applying the model "PAP". In *Electron Probe Quantitation* (eds. K. F. J. Heinrich and D. E. Newbury). Plenum Press, New York, NY, pp. 31–75.

Rubin A. E. (2004) Postshock annealing and postannealing shock in equilibrated ordinary chondrites: implications for the thermal and shock histories of chondritic asteroids. *Geochim. Cosmochim. Acta* **68**, 673–689.

Rubin A. E. (2010) Physical properties of chondrules in different chondrite groups: implications for multiple melting events in dusty environments. *Geochim. Cosmochim. Acta* **74**, 4807–4828.

Rubin A. E., Kallemeyn G. W., Wasson J. T., Clayton R. N., Mayeda T. K., Grady M., Verchovsky S., Eugster O. and Lorenzetti S. (2003). *Geochim. Cosmochim. Acta* **67**, 3283–3298.

Russell S. S., McCoy T. J., Rosewich E. and Ash R. D. (1998) The Burnwell, Kentucky, low iron oxide chondrite fall (1998). *Meteorit Planet. Sci.* **33**, 853–856.

Savage P. S. and Moynier F. (2013) Silicon isotopic variation in enstatite meteorites: clues to their origin and Earth-forming material. *Earth Planet. Sci. Lett.* **361**, 487–496.

Scott E. R. D. (1988) A new kind of primitive chondrite. *Earth Planet. Sci. Lett.* **91**, 1–18.

Stöffler D., Keil K. and Scott E. R. D. (1991) Shock metamorphism of ordinary chondrites. *Geochim. Cosmochim. Acta* **55**, 3845–3867.

Teplyakova S. N., Humayun M., Lorenz C. A and Ivanova M. A. (2012) A common parent for IIE iron meteorites and H chondrites. LPS, 43, abstract #1130.

Troiano J., Rumble, III, D., Rivers M. L. and Friedrich J. M. (2011) Compositions of three low- FeO ordinary chondrites: indications of a common origin with the H chondrites. *Geochim. Cosmochim. Acta* **75**, 6511–6519.

Van Niekirk D. and Keil K. (2011) Metal/sulfide–silicate intergrowth textures in EL3 meteorites: Origin by impact melting on the EL parent body. *Meteorit. Planet. Sci.* **46**, 1487–1494.

Warren P. H. (2011) Stable-isotopic anomalies and the accretionary assemblage of the Earth and Mars: A subordinate role for carbonaceous chondrites. *Earth Planet. Sci. Lett.* **311**, 93–100.

Wasson J. T. and Kallemeyn G. W. (1990) Allan Hills 85085: A subchondritic meteorite of mixed nebular and regolithic heritage. *Earth Planet. Sci. Lett.* **101**, 148–161.

Wasson J. T. and Scott E. R. D. (2011) Group IIE Iron meteorites: metal composition, formation, relationship to ordinary chondrites. LPSC, 42, Abstract #2813.

Wasson J. T. and Wang J. (1986) A nonmagmatic origin of group-IIE iron meteorites. *Geochim. Cosmochim. Acta* **50**, 725–732.

Weisberg M. K. and Kimura M. (2012) The unequilibrated enstatite chondrites. *Chem. Erde* **72**, 101–115.

Weisberg M. K., Prinz M. and Nehru C. E. (1988) Petrology of ALH85085: a chondrite with unique characteristics. *Earth Planet. Sci. Lett.* **91**, 19–32.

Weisberg M. K., Prinz M. and Nehru C. E. (1990) The Bencubbin chondrite breccia and its relationship to CR chondrites and the ALH 85085 chondrite. *Meteoritics* **25**, 269–279.

Weisberg M. K., Prinz M., Clayton R. N., Mayeda T. K., Grady M. M. and Pillinger C. T. (1995) The CR chondrite clan. *Proc. NIPR Symp. Antarct. Meteorit.* **8**, 11–32.

Weisberg M. K., Prinz M., Clayton R. N., Mayeda T. K., Sugiura N., Zashu S. and Ebihara M. (2001) A new metal-rich chondrite grouplet. *Meteorit. Planet. Sci.* **36**, 401–418.

Weisberg M. K., Bunch T. E., Rumble D. III and Ebel D. S. (2011a) Petrology and oxygen isotopes of NWA 5492, a new metal-rich chondrite. Lunar Planet. Sci. Lunar Planet. 42. Inst., Houston, # 1198 (abstr.).

Weisberg M. K., Ebel D. S., Connolly, Jr., H. C., Kita N. T. and Ushikubo T. (2011b) Petrology and oxygen isotope compositions of chondrules in E3 chondrites. *Geochim. Cosmochim. Acta* **75**, 6556–6569.

Weisberg M. K., Bunch T. E., Wittke J. H., Rumble, III, D. and Ebel D. S. (2012) Petrology and oxygen isotopes of NWA 5492, a new metal-rich chondrite. *Meteorit. Planet. Sci.* **47**, 363–373.

Young E. D. and Russell S. S. (1998) Oxygen reservoirs in the early solar nebula inferred from an Allende CAI. *Science* **282**, 452–455.

Zolensky M., Ziegler K., Weisberg M. K., Gounelle M. and Berger E. (2014) Aqueous Alteration of Enstatite Chondrites. Lunar Planet. Sci. 45 Lunar Planet. Inst., Houston, # 2116 (abstr.).

Associate editor: Anders Meibom